Blowup as a driving mechanism of turbulence in shell models

Alexei A. Mailybaev[*]

Instituto Nacional de Matemática Pura e Aplicada–IMPA, Rio de Janeiro, Brazil
(Received 2 March 2013; published 17 May 2013)

Since Kolmogorov proposed his phenomenological theory of hydrodynamic turbulence in 1941, the description of the mechanism leading to the energy cascade and anomalous scaling remains an open problem in fluid mechanics. Soon after, in 1949, Onsager noticed that the scaling properties in the inertial range imply nondifferentiability of the velocity field in the limit of vanishing viscosity. This observation suggests that the turbulence mechanism may be related to a finite-time singularity (blowup) of incompressible Euler equations. However, the existence of such blowup is still an open problem too. In this paper, we show that the blowup indeed represents the driving mechanism of the inertial range for a simplified (shell) model of turbulence. Here, blowups generate coherent structures (instantons), which travel through the inertial range in finite time and are described by universal self-similar statistics. The anomaly (deviation of scaling exponents of velocity moments from the Kolmogorov theory) is related analytically to the process of instanton creation using the large deviation principle. The results are confirmed by numerical simulations.

I. INTRODUCTION

Describing the mechanism of developed turbulence for the three-dimensional (3D) Navier-Stokes equations remains an important open problem in fluid mechanics. It encompasses various questions, and in this work we address the anomalous statistics of velocity moments in the inertial range and the dissipation anomaly (existence of finite dissipation in the inviscid limit). These questions remain a hot research topic since Kolmogorov presented the phenomenological theory of the inertial range in 1941 [1]. This theory of isotropic homogeneous turbulence leads to the power-law dependence of velocity moments on spatial scales, providing the scaling exponents $\zeta_p = p/3$ obtained on dimensional grounds. The exact scaling exponents deviate from the Kolmogorov theory. These deviations, called the anomalous corrections, are universal and become large with increasing p. Though a lot of knowledge is available now on the described anomalous phenomena, their mechanism is still not well understood [2,3].

In 1949, Onsager [4] related scaling properties of turbulent flow in the inertial range with the regularity of solutions obtained in the limit of vanishing viscosity. He conjectured that the anomalous turbulent dissipation requires the limiting velocity field to be nondifferentiable with the Hölder continuity exponent $h \leqslant 1/3$. This conjecture was proved later [5,6]. The irregularity of inviscid solutions allows for the consideration of the flow as a multifractal set with a continuous infinity of dimensions [2,7], which explains the nonlinear shape of scaling exponents ζ_p. Development of the theory of turbulence in this way includes the fundamental obstacle. It is the problem of blowup, i.e., the formation of a finite-time singularity in the incompressible 3D Euler equations from smooth initial data of finite energy. So far, the existence of blowup remains an open problem [8].

Simplified models help in understanding the turbulence phenomena. In this respect, the Gledzer-Ohkitani-Yamada

(GOY) shell model of turbulence [9,10] was successful in describing several nontrivial properties including the inertial range with anomalous dissipation and scaling. Shell models represent the dynamics in terms of characteristic (shell) velocities corresponding to a discrete set of wave numbers increasing in geometric progression and allow reliable numerical simulation at very high Reynolds numbers. The Sabra shell model proposed in [11] is characterized by improved regularity in the inertial range. Despite the large effort [12], the theory of turbulence for shell models, which would follow directly from the model equations and describe the observed statistics, is not yet accessible. On the other hand, the problem of blowup was recently formalized [13] and understood [14,15]. The blowup in the Sabra shell model has a self-similar universal structure [16]. The possible relation of such structure to the statistics of turbulence was discussed in [17,18]. Cascade models of turbulence [19] represent the extended version of shell models, where each shell is described by a large (though fixed) number of variables. These models lead to anomalous intermittent dynamics [20], and the universal self-similar blowup was observed numerically in the inviscid cascade model [21]. See also [18,22–24] for other numerical observations of self-similar blowup in shell models.

In this paper, we establish a direct link between the blowup and the turbulent dynamics in the inertial range for the Sabra shell model. We show that the blowuplike structures dominate the turbulent fluctuations and can be described as a "gas" of instantons. The instantons (coherent structures of shell velocities, which traverse the inertial range in the direction of large wave numbers) are represented and analyzed in terms of velocity local maxima. The striking property of instantons is that they maintain the universality and self-similarity of blowup, though with slightly different scaling exponents and in a statistical sense. This statistical universality of instantons was observed earlier in [25]. Then we show that instanton creation is the main process driving the inertial range dynamics. This allows derivation of the probability density function (PDF) for instanton amplitudes explicitly in terms of the anomalous scaling exponents ζ_p by using the large deviation principle. The obtained results fully agree with numerical simulations

_____

[*]Present address: Estrada Dona Castorina 110, 22460-320 Rio de Janeiro, RJ, Brazil. E-mail address: alexei@impa.br

and are also confirmed analytically for a class of instanton creation models. Finally, we discuss some qualitative changes in the turbulent regime, which occur with a change of model parameter.

The paper is organized as follows. Section II introduces the Sabra shell model. The blowup universal properties in the inviscid model are described in Sec. III. In Sec. IV, we consider the statistics of maxima of velocity amplitudes and introduce a way to identify the instantons. Section V describes the universal self-similar statistics of instantons. In Sec. VI, we find universal expressions for PDFs of instantons using the large deviation principle. Section VII presents the analytical theory for a specific class of instanton creation models. Section VIII describes a different turbulent regime, which is dominated by a single blowup. The results are summarized in Sec. IX.

II. MODEL

In shell models of turbulence, the Fourier space is represented by a series of shells $n = 0, 1, 2, \ldots$, corresponding to wave numbers $k_n = \lambda^n$ with $\lambda = 2$. We consider the Sabra shell model [11]

$$\frac{du_n}{dt} = i[k_{n+1}u_{n+2}u_{n+1}^* - (1+c)k_n u_{n+1}u_{n-1}^* \\ - ck_{n-1}u_{n-1}u_{n-2}] - \nu k_n^2 u_n + f_n, \quad (1)$$

where u_n is the complex shell velocity, which can be understood as the Fourier component of the velocity field at the shell wave number k_n, $\nu \geqslant 0$ is the viscosity, and c is the parameter controlling nonlinear coupling of the shells. The terms f_n model external forces at large scales and, thus, they are usually restricted to the first few shells. The inviscid system with no forcing ($\nu = f_n = 0$) conserves the energy $E = \frac{1}{2}\sum_n |u_n|^2$. The second quadratic invariant $H = \sum_n c^{-n}|u_n|^2$ is associated with the helicity for $c = -0.5$ when $c^{-n} = (-1)^n k_n$. Additionally, there are four symmetry transformations:

$$t \mapsto t - t_0; \quad (2)$$

$$u_n \mapsto e^{i\theta_n}u_n, \quad \theta_n = \theta_{n-1} + \theta_{n-2}; \quad (3)$$

$$t \mapsto t/a, \quad u_n \mapsto au_n; \quad (4)$$

$$u_n \mapsto \lambda u_{n+1}. \quad (5)$$

Here, Eqs. (2) and (3) can be associated with the time and physical space translations, while Eqs. (4) and (5) correspond to the time and space scaling; see [12].

III. BLOWUP IN INVISCID MODEL

Let us consider solutions $u_n(t)$ with the finite norm $|u|_1 < \infty$ defined as

$$|u|_1 = \left(\sum_n k_n^2 |u_n|^2\right)^{1/2}. \quad (6)$$

The blowup represents a singularity given by

$$|u|_1 \to \infty \quad \text{as} \quad t \to t_c^-, \quad (7)$$

which develops in finite time $t_c < \infty$ from the initial condition of the finite norm [13]. Note that the singularity is described by the norm, while each particular shell speed $u_n(t)$ remains finite and smooth. This reflects the fact that the shell model corresponds to dynamics in the Fourier space, where the condition such as (7) implies the divergence of velocity derivatives in physical space, i.e., infinite vorticity. The blowup is only possible in the inviscid shell model, and the uniqueness of the solution is insured only for $t < t_c$ [13].

Let us consider the inviscid model with vanishing forcing terms, $\nu = f_n = 0$. Then we write Eq. (1) as

$$\frac{du_n'}{dt} = N_n[u'], \quad u_n' = ik_n u_n, \quad (8)$$

with the quadratic nonlinearity

$$N_n[u'] = -\lambda^{-2}u_{n+2}'u_{n+1}'^* + (1+c)u_{n+1}'u_{n-1}'^* - c\lambda^2 u_{n-1}'u_{n-2}'. \quad (9)$$

Following the approach suggested by Dombre and Gilson [14] (see also [16]), we consider the renormalized time τ and shell speeds w_m introduced as

$$t = t_0 + \int_0^\tau \exp\left[-\int_0^{\tau'} A(\tau'')d\tau''\right]d\tau', \\ u_n' = \exp\left[\int_0^\tau A(\tau')d\tau'\right]w_n, \quad (10)$$

where $\tau = 0$ corresponds to the initial time t_0 and $A(\tau)$ is specified below. It is straightforward to check that

$$\frac{dw_n}{d\tau} = N_n[w] - Aw_n, \quad (11)$$

where $N_n[w]$ has the form (9) written in terms of w_n instead of u_n'. One can also check that Eq. (11) conserves the sum $\sum |w_n|^2$ if we choose

$$A(\tau) = \text{Re}\sum_n w_n^* N_n[w] \Big/ \sum_n |w_n|^2. \quad (12)$$

The idea of the above transformation is that Eq. (11) admits an asymptotic traveling wave solution of the form [14]

$$w_n(\tau) = W(n - s\tau), \quad (13)$$

where s is the wave speed and $W(\xi)$ is a function vanishing as $\xi \to \pm\infty$. This traveling wave exists for a large range of shell model parameter c, and it is determined up to symmetries induced by Eqs. (2)–(5). For the original shell speeds $u_n(t)$ related to $w_n(\tau)$ by Eqs. (8) and (10), solution (13) yields [14,16]

$$u_n(t) = -ik_n^{-y_0}U[k_n^{z_0}(t - t_c)], \quad (14)$$

where

$$U(t - t_c) = \exp\left[\int_0^\tau A(\tau')d\tau'\right]W(-s\tau), \quad (15)$$

$$z_0 = \frac{1}{\log\lambda}\int_0^{1/s} A(\tau)d\tau, \quad y_0 = 1 - z_0, \quad (16)$$

$$t_c = t_0 + \int_0^\infty \exp\left[-\int_0^{\tau'} A(\tau'')d\tau''\right]d\tau'. \quad (17)$$
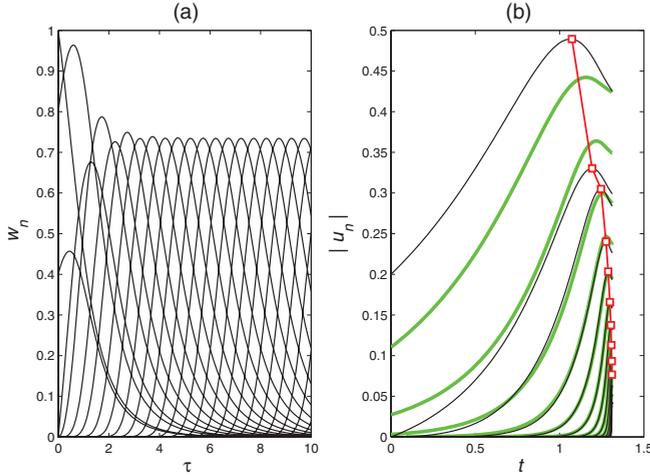
FIG. 1. (Color online) (a) Traveling wave formation in the dynamics of the renormalized inviscid Sabra model. Shown are the curves $w_n(\tau)$ with $n = 0, 1, \ldots$ increasing from the left to the right. (b) The corresponding dynamics of shell speeds $u_n(t)$ for $n = 2, 3, \ldots$. Bold green (light gray) curves show the universal self-similar asymptotic form of blowup. Red squares indicate the correlated sequence of maxima $v_n = \max_t |u_n(t)|$.

If $y_0 < 1$, then Eq. (14) describes the asymptotic form of blowup at finite time $t_c < \infty$. In this asymptotic form, y_0 is the universal scaling exponent independent of initial conditions, and the function $U(t)$ describes the universal self-similar shape of the blowup given up to the scaling symmetry of the Sabra model. The equality $y_0 + z_0 = 1$ reflects the dimensional relation $t_n - t_c \propto (v_n k_n)^{-1}$, where $v_n = \max_t |u_n(t)|$ and t_n is the corresponding time. For details of the derivations and the rigorous theory, which associate the traveling wave (13) with a fixed-point attractor of the Poincaré map, see [15].

As an example, let us consider the case $c = -0.5$. The solution $w_n(\tau)$ of the renormalized system (11) for real initial conditions is shown in Fig. 1(a). One can clearly see the formation of the traveling wave solution (13). The solution for the original shell speeds $u_n(t)$ is presented in Fig. 1(b), which blows up at finite time $t \to t_c$ given by Eq. (17). Using Eqs. (15) and (16), we compute the scaling exponent $y_0 = 0.281$ and the function $U(t)$. The bold green curves in Fig. 1(b) show the asymptotic self-similar solution (14) for the blowup, and one can readily see the convergence. Numerical analysis confirms asymptotic stability of the traveling wave solution in Fig. 1(a) due to both real and complex perturbations. As we already mentioned, this implies that Eq. (14) provides the universal asymptotic form of blowup.

Similar traveling wave solutions exist for $c < -0.092$. The corresponding scaling exponent y_0 and function $U(t)$ are shown in Fig. 2. The function $U(t)$ is monotonous for $c < -0.671$, possesses a single extremum (maximum) for $-0.671 < c < -0.139$, and has several extrema for $-0.139 < c < -0.092$. At $c = -0.139$, we have $U(0) = 0$ and the scaling exponent attains the minimum $y_0 = 0$. This fact can be understood using the energy conservation argument. Indeed, y_0 in Eq. (14) cannot be negative, otherwise the shell speeds and the energy would grow infinitely. In the case $y_0 = 0$, all of the energy is transported to large shells as $t \to t_c^-$, so that
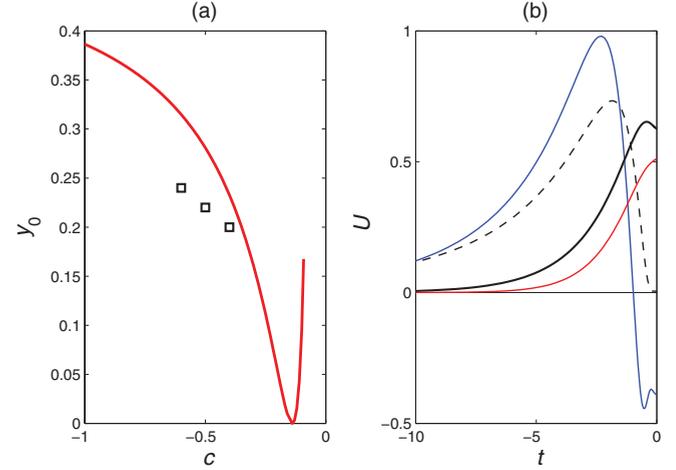
FIG. 2. (Color online) (a) Dependence of the blowup scaling exponent y_0 on the Sabra model parameter c. Squares show the scaling exponents y of instantons. (b) The universal function $U(t)$ in the asymptotic expression (14) for $c = -0.1$ (upper curve, blue), $c = -0.139$ (dotted curve), $c = -0.5$ (solid black curve), and $c = -1$ (lower curve, red).

no energy remains in each shell at the time of blowup, i.e., $U(0) = 0$.

The real traveling wave solution (13) becomes unstable with respect to complex perturbations at the critical value $c = -0.092$. For $c > -0.092$, analysis of the blowup requires more sophisticated techniques (see [15]), which are beyond the scope of this paper.

IV. INSTANTONS IN INERTIAL RANGE OF TURBULENT REGIME

It is known that for the parameter $c = -0.5$, the Sabra model with small viscosity (large Reynolds number) demonstrates chaotic intermittent behavior. The statistical properties of this system have much in common with the developed turbulence of the 3D Navier-Stokes equations [11]. In particular, it possesses a wide (increasing with the Reynolds number) inertial range of wave numbers k_n separating the scales influenced by forcing (small k_n) and the scales dominated by viscosity (large k_n). This inertial range is responsible for the energy cascade, i.e., the flux of energy produced in the forcing range by external forces to the viscous range, where it is dissipated due to viscosity. The existence of a positive limit of mean dissipation rate for infinite Reynolds numbers constitutes the famous dissipation anomaly of turbulent hydrodynamic flows.

The important quantitative characteristic of the inertial range is given by the structure functions (velocity moments). In the inertial range, these functions depend on k_n as power laws,

$$S_p(k_n) = \langle |u_n|^p \rangle \propto k_n^{-\zeta_p}. \tag{18}$$

In this expression, p is an arbitrary real number; traditionally, the computations are carried out for positive integer values of p. The scaling exponents ζ_p are universal, i.e., they are independent both of the forcing and viscosity. Figure 3 presents the functions $S_p(k_n)$ in logarithmic coordinates for
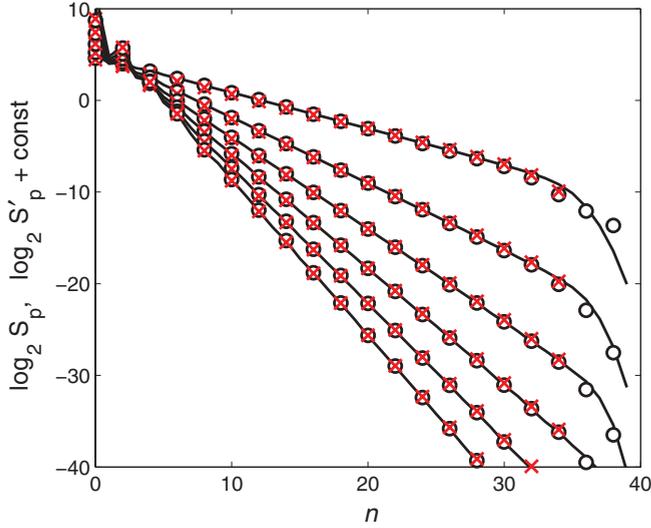
FIG. 3. (Color online) Solid black lines present the velocity moments $S_p(k_n) = \langle |u_n|^p \rangle$ for $p = 1, \ldots, 6$. Black circles determine the functions $S'_p(k_n)$ from Eq. (19); for a better comparison of slopes, the graphs are shifted in the vertical direction and only even n are shown. Red crosses show similar functions $S'_p(k_n)$ computed for the local maxima v_n corresponding to stable instantons only. Three types of structure functions determine equal slopes in the inertial range given by the scaling exponents $-\zeta_p$.

the Sabra model with $c = -0.5$. These results are based on direct numerical simulation of Eq. (1) with 40 shells, viscosity $\nu = 10^{-14}$, and the constant forcing at the first two shells, $f_0 = 1 + i$ and $f_1 = f_0/2$. One can clearly distinguish the forcing range corresponding roughly to the shells $n \leqslant 5$, the viscous range of shells $n \geqslant 32$, and the linear part in between indicating the inertial range.

The phenomenological theory developed by Kolmogorov (K41 [1,2]) predicts the linear dependence $\zeta_p = p/3$ for the scaling exponents. However, the exact scaling exponents ζ_p depend nonlinearly on p. This deviation from the K41 theory is called the anomaly. The scaling exponents are presented in Fig. 4. The two exact values of scaling exponents are known. The first one is $\zeta_0 = 0$ since $|u_n|^0 = 1$. The second exact exponent is $\zeta_3 = 1$, which is a necessary condition for the dissipation anomaly; see, e.g., [11]. The scaling exponents of the 3D Navier-Stokes turbulence are close to the ones given by the Sabra model [2,11].

In this section, we establish a link between the anomalous turbulent statistics and the blowup phenomenon for the Sabra shell model. The blowup analysis of the inviscid model is relevant in the inertial range, where viscosity is insignificant. However, there is an essential difference related to initial conditions. For the blowup considered in Sec. III, finiteness of the norm (6) requires decay of initial shell speeds faster than k_n^{-1}. This condition is violated in the inertial range of developed turbulence, which is characterized by the power-law decay (18) with $\zeta_1 \approx 0.39$. We will see that this difference leads to the transformation of the blowup with universal self-similar asymptotic form to coherent structures with universal self-similar statistics.

Identification of these coherent structures in the turbulent regime is strongly facilitated, if we consider local maxima
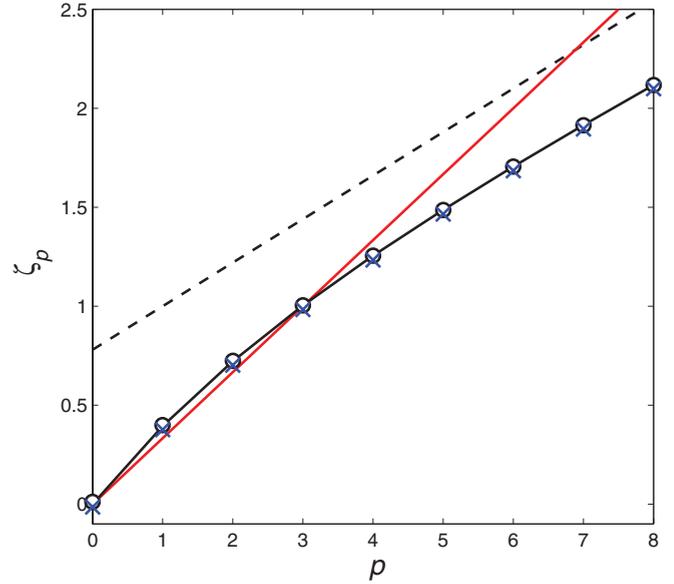
FIG. 4. (Color online) Anomalous scaling exponents ζ_p computed for the velocity moments S_p (black line) and for the functions S'_p (circles and crosses correspond to the sums over all maxima and over maxima from stable instantons, respectively). The red (gray) line $\zeta_p = p/3$ corresponds to the phenomenological K41 theory. The dotted line shows the upper bound (28) based on the instanton scaling.

$v_n = \max_t |u_n(t)|$ of shell speed amplitudes. An extra subscript is necessary to index all the local maxima in shell n, but we will drop it for the sake of simplicity of notations. The new "structure" functions are defined as

$$S'_p(k_n) = \frac{1}{T k_n} \sum v_n^{p-1}, \qquad (19)$$

where the sum is taken over all local maxima v_n observed for the speed amplitude $|u_n(t)|$ during a large time interval $0 \leqslant t \leqslant T$. By a simple dimensional consideration, one finds that each local maximum v_n has the characteristic time $\Delta t_n \sim (k_n v_n)^{-1}$ determining the time interval, where $|u_n(t)| \sim v_n$. For the velocity moment $\langle |u_n|^p \rangle = T^{-1} \int_0^T |u_n|^p dt$, this yields the contribution of order

$$T^{-1} v_n^p \Delta t_n = (T k_n)^{-1} v_n^{p-1}, \qquad (20)$$

leading naturally to Eq. (19). Hence, the functions S'_p are expected to scale in the same way as S_p in the inertial range, i.e.,

$$S'_p(k_n) \propto k_n^{-\zeta_p}, \qquad (21)$$

with the same scaling exponents as in Eq. (18). This hypothesis perfectly agrees with the numerical simulations as shown in Figs. 3 and 4.

The blowup in the inviscid shell model can be identified as the correlated sequence of maxima, which follow in increasing order of n and t; see Fig. 1. Analogous correlated structures (called the instantons) are observed in the inertial range of shell models [17,18,26]; see Fig. 5. Following [25], we identify the instanton as a sequence of local maxima $v_n = \max_t |u_n(t)|$ at times t_n following in increasing order $t_{n_0} \leqslant t_{n_0+1} \leqslant \cdots \leqslant t_{n_1}$. In this definition, no maxima of $|u_n(t)|$ or $|u_{n+1}(t)|$ are allowed in the interval $t_n < t < t_{n+1}$. Each instanton is created
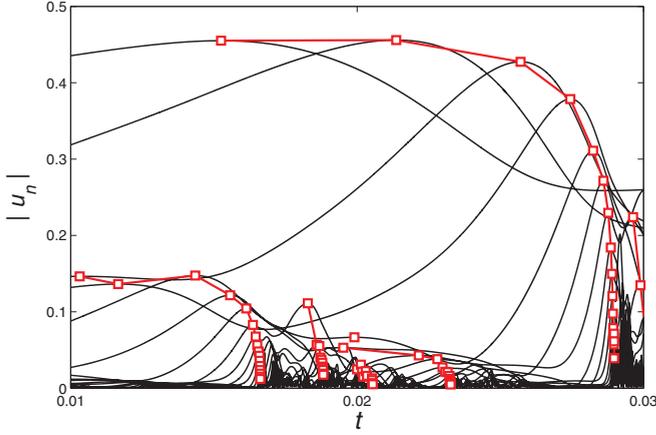
FIG. 5. (Color online) Typical dynamics of speed amplitudes $|u_n(t)|$ shown for the shells $n = 7, \ldots, 24$. Red squares mark correlated sequences of local maxima (instantons), which have a structure similar to the blowup in Fig. 1. Shown are the instantons created in shells $n_0 = 7, \ldots, 14$.

at some shell number n_0 and either reaches the viscous range or annihilates at a shell number n_1 in the inertial range. Using this rule, we group all maxima of velocity amplitudes into instantons; see Fig. 5.

As we already mentioned, an instanton can be viewed as a blowup deformed by the inertial range environment in which it propagates. One can see from Fig. 5 that this deformation is caused, mostly, by interaction with adjacent instantons. Let N_{all} be the number of all maxima v_n in a given shell n. Figure 6(a) provides numerical values for the relative number N/N_{all}, where N is the number of maxima in shell n corresponding to a specified type of instantons. Most of the maxima correspond to stable instantons, which reach the viscous range, i.e., in our simulation $n_1 \geqslant 32$. These instantons cover from 60 to 90% of the total number of maxima in a given shell n [bold black line in Fig. 6(a)]. The majority of the remaining maxima (about 20%) belong to very short instantons with $n_1 \approx n_0$, which can be considered as uncorrelated fluctuations. The instantons annihilating after traversing more than two shells but before the viscous range are rare.

We see that the turbulent dynamics in the inertial range of the Sabra model has the highly correlated structure, where the blowup plays the role of the driving mechanism. Another evidence supporting our observation is obtained if we compute the scaling exponents ζ_p for the functions (19), where only the maxima from stable instantons are included in the sum. These results are shown by crosses in Figs. 3 and 4. The same scaling exponents as for the velocity moments (18) are obtained (a tiny difference in Fig. 4 is the same for all p and, thus, corresponds to a small change of the total number of maxima included in the sum). In the following analysis, we will consider only the maxima belonging to stable instantons in the sum (19).

Description of the inertial range in terms of instantons provides an alternative interpretation of the first scaling exponent ζ_1. Let M_n be the average number of stable instantons created in shell n per unit time. Using Eqs. (19) and (21), we
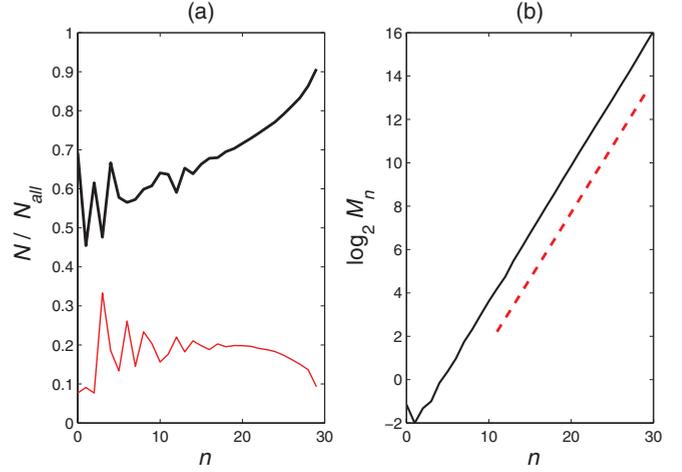
FIG. 6. (Color online) (a) The number N of selected local maxima in the shell n relative to their total number N_{all}. The bold black line corresponds to the maxima chosen from stable instantons. The thin red (lower) line corresponds to uncorrelated maxima (instantons of length 1 or 2). (b) Power-law scaling for the number M_n of stable instantons created in shell n per unit time. The slope $1 - \zeta_1$ is shown by the dotted line.

have

$$S_1'(k_n) = \frac{1}{T k_n} \sum 1 = \frac{1}{k_n} \sum_{m=0}^{n} M_m \propto k_n^{-\zeta_1}, \qquad (22)$$

where the first sum counts the maxima of stable instantons in shell n. It is easy to check that Eq. (22) implies

$$M_n \propto k_n^{1-\zeta_1}. \qquad (23)$$

We found that ζ_1 determines the power-law scaling for the number of instantons created in shell n. For the Sabra model with $c = -0.5$, we have $1 - \zeta_1 = 0.61$, which is in very good agreement with numerical data; see Fig. 6(b).

The scaling exponent $\zeta_0 = 0$ is a simple consequence of the equality $\langle |u_n|^0 \rangle = 1$. However, this exponent gets nontrivial interpretation in terms of velocity maxima in Eq. (19) written as

$$S_0'(k_n) = \frac{1}{T k_n} \sum v_n^{-1} \sim \frac{1}{T} \sum \Delta t_n, \qquad (24)$$

where, as we showed earlier, $\Delta t_n \sim (k_n v_n)^{-1}$ is the characteristic time associated with the maximum v_n. Relation $S_0' \propto k_n^{\zeta_0} = 1$ implies that the total fraction of time occupied by these maxima is finite for each shell, i.e., the stable instantons are dense in space-time.

Numerical simulations for the model with the parameter values $c = -0.4$ and -0.6 were also carried out. The results are very similar to those presented in Figs. 3–6, which confirm our conclusion about the role of instantons as principal elements of turbulent dynamics in the inertial range of the Sabra model.

V. SELF-SIMILAR STATISTICS OF INSTANTONS

The universal self-similarity of blowup (14) is destroyed in the turbulent regime due to chaotic emergence and interaction of instantons; see Fig. 5. The most striking property of the

instantons is that they restore the blowup self-similarity in a statistical sense in the inertial range. To observe this property, let us consider the functions

$$R_p^{(n_0)}(k_n) = \frac{1}{T} \sum_{(n_0)} v_n^p, \quad n \geqslant n_0, \quad (25)$$

where the sum is taken over the local maxima belonging to stable instantons created in fixed shell n_0. These functions can be viewed as effective velocity moments for the instantons born in a specific shell, and their graphs obtained numerically are shown in Fig. 7(a) in logarithmic coordinates. One can clearly see that the functions $R_p^{(n_0)}$ obey the power-law scaling with exponents (slopes) independent of the initial shell number n_0.

The next observation is that the slopes of the graphs in Fig. 7(a) are proportional to p. This is shown in Fig. 7(b), where the functions $(1/p) \log_2 R_p^{(n_0)}$ are plotted versus a number of shells $n - n_0$ traversed by the instanton. All curves (after the vertical shift) collapse onto a single straight line of slope $-y$ with $y \approx 0.22$. This implies the relation

$$R_p^{(n_0)}(k_n) = c_p^{(n_0)} \lambda^{-py\Delta n} \propto k_{\Delta n}^{-py}, \quad \Delta n = n - n_0 \geqslant 0, \quad (26)$$

with the universal value of scaling exponent y in the inertial range. The scaling exponent $y \approx 0.22$ is different but close to the scaling exponent $y_0 \approx 0.281$ of the blowup; see Fig. 2(a).

The scaling rule in Eq. (26) suggests the universal self-similarity of instanton statistics. Let us consider the probability density functions (PDFs) determining the probability $P_{n_0,n}(v) dv$ to sample a local maximum $v = \max_t |u_n(t)|$ belonging to the instanton created in shell n_0. The self-similarity for PDFs implies that the renormalized function

$$P_{n_0}(v) = \lambda^{-y\Delta n} P_{n_0,n}(\lambda^{-y\Delta n} v) \quad (27)$$

does not depend on n in the inertial range. This hypothesis fully agrees with the numerical results as one can see in

FIG. 8. (Color online) Renormalized PDFs $P_{n_0}(v)$ of instantons found numerically for $n_0 = 17$ and $n = 17, \ldots, 29$ (thin black curves) and for $n_0 = 20$ and $n = 20, \ldots, 29$ (thin blue curves). Collapse of the graphs with fixed n_0 onto a single curve confirms the self-similarity of PDFs in the inertial range. Bold dotted curves show the PDFs determined by the large deviation principle.

Fig. 8(a), where the functions (27) for different n collapse onto a single curve for fixed $n_0 = 17$ or 20. The functions $P_{n_0}(v)$ for different n_0 are related by the large deviation principle, as we will show in the next section.

We conclude that the instantons created in a given shell possess self-similar statistics. These instantons can be viewed as the blowup phenomena, which propagate to the viscous range interacting with each other. Interaction is an important factor which leads to a small but finite difference between the scaling exponent of the instanton $y \approx 0.22$ and the scaling exponent of the blowup $y_0 \approx 0.28$. Similar results are obtained for the Sabra model with the parameters $c = -0.4$ and -0.6. The corresponding values of scaling exponents y are shown in Fig. 2(a).

VI. LARGE DEVIATION PRINCIPLE FOR INSTANTON DISTRIBUTIONS

According to Eqs. (19), (25), and (26), an average contribution of a single instanton to the function $S_p'(k_n)$ is proportional to $k_n^{-1-(p-1)y}$. This yields an upper bound for the scaling exponents in Eq. (21) as

$$\zeta_p \leqslant 1 + (p-1)y. \quad (28)$$

The dotted line in Fig. 4 represents the right-hand side of Eq. (28). Since the graph of ζ_p is a concave function [2], we conclude that the instanton scaling exponent y does not determine any part of the ζ_p graph. In particular, $y \approx 0.22$ is larger than the slope of the ζ_p graph for large p (the numerical data provides the slope $d\zeta_p/dp$ decreasing below 0.19). Therefore, the instanton scaling does not determine the scaling of high-order velocity moments, as was conjectured

FIG. 7. (Color online) (a) The functions $R_p^{(n_0)}(k_n)$ in logarithmic coordinates demonstrating power-law scaling of instantons. Curves of the same color correspond to the instantons created in shells $n_0 = 13, \ldots, 23$. Different colors indicate different values of $p = 1, \ldots, 6$ from top to bottom. (b) Graphs of the left figure collapse onto a single straight line when divided by p. The slope $-y$ is shown by the dotted line.

in [18] (however, this becomes true for different values of the model parameter c, as we show in Sec. VIII).

The anomalous exponents ζ_p arise in the process of instanton creation. In order to see this, we use relations (19), (25), and (26) and find

$$S'_p(k_n) = k_n^{-1} \sum_{n_0=0}^{n} R_{p-1}^{(n_0)}(k_n)$$

$$= k_n^{-1} \sum_{n_0=0}^{n} c_{p-1}^{(n_0)} \lambda^{-(p-1)y(n-n_0)}. \qquad (29)$$

Then the coefficients are expressed from (29) as

$$c_{p-1}^{(n)} = k_n S'_p(k_n) - \lambda^{-(p-1)y} k_{n-1} S'_p(k_{n-1}). \qquad (30)$$

In the inertial range, where the power-law scaling (21) holds, we have

$$c_{p-1}^{(n)} \propto k_n^{1-\zeta_p}. \qquad (31)$$

This relation was also confirmed numerically. We see that due to the self-similar structure of instantons, anomalous scaling is attributed exclusively to the coefficients $c_p^{(n_0)}$ describing amplitudes of instantons created in shell n_0. This property relates the inertial range anomaly with the process of instanton creation.

Relation (31) allows one to find the universal form of PDFs $P_n(v)$ in Eq. (27) as follows. Using Eqs. (25)–(27), we obtain

$$c_{p-1}^{(n)} = R_{p-1}^{(n)}(k_n) = \frac{1}{T} \sum_{(n)} v_n^{p-1} = M_n \int_0^\infty v^{p-1} P_{n,n}(v) dv$$

$$= M_n \int_0^\infty v^{p-1} P_n(v) dv, \qquad (32)$$

where M_n is the number of instantons created in shell n per unit time. Introducing the new variable a and function $\rho(a)$ as

$$a = \frac{1}{n} \log_\lambda \frac{v}{v_*}, \quad \rho_n(a) = \rho_* n M_n P_n(v), \qquad (33)$$

where v_* and ρ_* are constant coefficients, we write Eq. (32) in the form

$$c_{p-1}^{(n)} = \frac{v_*^p}{\rho_*} \log \lambda \int \lambda^{npa} \rho_n(a) da. \qquad (34)$$

Using Eq. (31), we find the power-law scaling rule for the integral in the right-hand side as

$$\int \lambda^{npa} \rho_n(a) da \propto k_n^{1-\zeta_p} = \lambda^{n(1-\zeta_p)}. \qquad (35)$$

In Eq. (35), the scaling exponent $1 - \zeta_p$ is a smooth convex function of $p \in \mathbb{R}$; see Fig. 4. Hence, we can apply the Gärtner-Ellis theorem [27–29] to Eq. (35), which states that $\rho_n(a)$ has the asymptotic form

$$\rho_n(a) \propto \lambda^{-nJ(a)} = k_n^{-J(a)} \qquad (36)$$

for large n, where the rate function $J(a)$ is the Legendre transform of the function $1 - \zeta_p$, i.e.,

$$J(a) = pa - (1 - \zeta_p), \quad a = -\frac{d\zeta_p}{dp}. \qquad (37)$$
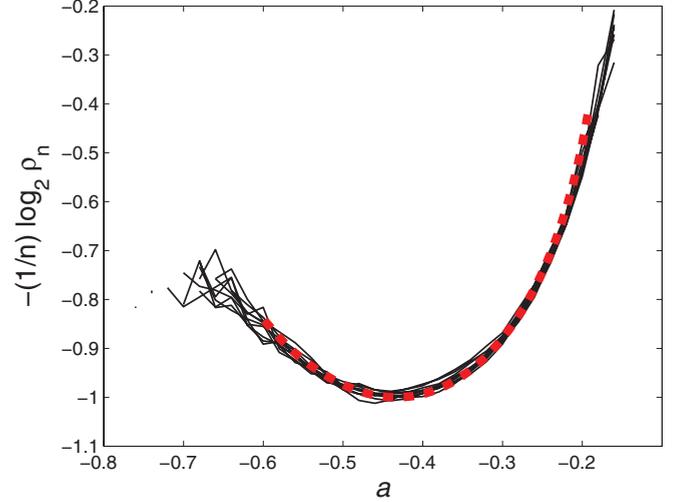
FIG. 9. (Color online) The functions $-(1/n)\log_\lambda \rho_n$ computed numerically for $n = 17, \ldots, 26$ (thin black lines) are compared with the rate function $J(a)$ (dotted red line).

Expression (36) is called the large deviation principle. Note that the Gärtner-Ellis theorem is formulated for $\lambda = e$, but one can easily check its validity for any $\lambda > 1$.

We verify Eq. (36) in Fig. 9, where the black curves show the functions $-(1/n)\log_\lambda \rho_n(a)$ found numerically using Eqs. (27) and (33) for $n = 17, \ldots, 26$ and $n_0 = n$. As expected, these graphs collapse onto a single curve given by the rate function $J(a)$. The rate function represented by the red dotted line was computed using the Legendre transform (37) for the scaling exponent ζ_p in the interval $-2 \leqslant p \leqslant 10$. In numerical computations, it was important to choose good values of the constants v_* and ρ_* in Eq. (33) in order to achieve better convergence.

The final result of our derivation is obtained by substituting Eq. (36) into (33) as

$$M_n P_n(v) \propto k_n^{-J(a)}, \quad a = \frac{1}{n} \log_\lambda \frac{v}{v_*}, \qquad (38)$$

where we dropped the factor n^{-1} representing a logarithmic correction for the first expression. Note that the asymptotic form given by the Gärtner-Ellis theorem in Eq. (36) is understood as $n^{-1} \log_\lambda \rho_n(a) \to -J(a)$ in the limit $n \to \infty$. Recall that the same limit of large n is used in the definition of inertial range, which corresponds to shell numbers far from the forcing range. Thus, Eq. (38) is valid in the inertial range. This statement is confirmed numerically in Fig. 8, where the asymptotic PDFs given by Eq. (38) are shown by the dotted red curves for the shells 17 and 20 (with the constant factors properly adjusted).

We showed that the PDFs of instantons in the inertial range have the universal self-similar form (38) related to the anomalous scaling exponents by Eqs. (37). Thus, the instantons satisfy the large deviation principle leading to the inertial range anomaly. The presented analysis has much in common with the phenomenological model of multifractality [2]. In this model, it is assumed that the velocity field can be decomposed into fractal subsets with different scaling properties, and the fractal dimensions are related to the

anomalous exponents ζ_p by the Legendre transform. However, the fractal subsets in the multifractal model are hard to define and detect numerically or experimentally, as well as to justify their appearance. On the contrary, the presented approach based on the study of instantons is related to the analytical theory of blowup and is supported by the detailed numerical analysis.

VII. INSTANTON CREATION MODEL

In this section, we introduce a phenomenological model for instanton creation, where the large deviation principle can be derived analytically. As one can see in Fig. 5, an instanton traveling through the inertial range leaves a trace (energy) in all of the shells it passed through. Due to the asymptotic stability of blowup mentioned in Sec. III, this energy "feeds" a series of newly created instantons in different shells. This process leads to the formation of a "gas" of instantons, which is dense in space-time and carries the energy from the forcing to the viscous range. As the viscosity plays no role in this process, the dissipation anomaly becomes a natural consequence of the described behavior.

In this phenomenological picture, instantons create other instantons. A simple statistical model of the creation process can be developed as follows. We assume that an instanton, which reaches the shell n with the amplitude $v_n = 1$, creates on average $\varphi(v)dv$ new instantons of amplitude $v_n = v$ in this shell. Here, $\varphi(v)$ is the creation rate function, which is assumed to be universal, i.e., independent of n. For an instanton of arbitrary amplitude $v_n = v'$, the density of created instantons is given by

$$\frac{1}{v'} \varphi\left(\frac{v}{v'}\right) dv, \tag{39}$$

as it follows from the scaling symmetry of the Sabra model. As before, we consider only stable instantons, which cover up to 90% of all shell oscillations [Fig. 6(a)], and disregard other types of fluctuations.

Using the definitions of Sec. V, the distribution of instanton amplitudes is described by the product

$$M_n P_{n,n}(v)dv, \tag{40}$$

determining a number of instantons with maxima $v_n = v$ created in shell n per unit time. Here, $P_{n,n}$ is the PDF of such instantons and M_n is the total instanton creation rate in shell n. Distribution of maxima $v_n = v$ corresponding to the instantons created in previous shells $n_0 < n$ is found similarly as

$$\sum_{n_0=0}^{n-1} M_{n_0} P_{n_0,n}(v)dv. \tag{41}$$

Using expressions (40) and (41), the instanton creation principle described by Eq. (39) yields

$$M_n P_{n,n}(v) = \int_0^\infty \left[\sum_{n_0=0}^{n-1} M_{n_0} P_{n_0,n}(v') \right] \frac{1}{v'} \varphi\left(\frac{v}{v'}\right) dv'. \tag{42}$$

Using Eq. (27), we write this expression as

$$M_n P_n(v) = \sum_{n_0=0}^{n-1} \int_0^\infty \lambda^{y(n-n_0)} M_{n_0} P_{n_0}(\lambda^{y(n-n_0)} v') \frac{1}{v'} \varphi\left(\frac{v}{v'}\right) dv'. \tag{43}$$

Let us compute the quantity (32) represented as

$$c_p^{(n)} = \int_0^\infty v^p M_n P_n(v) dv. \tag{44}$$

Expressing $M_n P_n$ from Eq. (43) and denoting $\xi = v/v'$ and $\eta = \lambda^{y(n-n_0)} v'$, we find

$$c_p^{(n)} = \sum_{n_0=0}^{n-1} \lambda^{-yp(n-n_0)} \iint_0^\infty (\eta\xi)^p M_{n_0} P_{n_0}(\eta) \varphi(\xi) \, d\xi \, d\eta. \tag{45}$$

Using Eq. (44) for $c_p^{(n_0)}$, the right-hand side of Eq. (45) is integrated as

$$c_p^{(n)} = \varphi_p \sum_{n_0=0}^{n-1} \lambda^{-yp(n-n_0)} c_p^{(n_0)}, \tag{46}$$

where

$$\varphi_p = \int_0^\infty \xi^p \varphi(\xi) d\xi. \tag{47}$$

Using Eq. (46) for $c_p^{(n)}$ and $c_p^{(n-1)}$, we compute the following difference:

$$c_p^{(n)} - \lambda^{-yp} c_p^{(n-1)} = \varphi_p \lambda^{-yp} c_p^{(n-1)}, \tag{48}$$

and obtain

$$c_p^{(n)} = \lambda^{-yp}(1 + \varphi_p) c_p^{(n-1)}. \tag{49}$$

Expression (49) implies the power law (31) with the exponents

$$\zeta_p = 1 + (p - 1)y - \log_\lambda(1 + \varphi_{p-1}). \tag{50}$$

Since $\varphi_{p-1} > 0$, this expression satisfies the inequality (28).

We determined the scaling exponents ζ_p explicitly in terms of the moments of the creation rate function $\varphi(v)$. For a particular example, when the creation rate is given by self-similarity arguments, this computation was done in [25]. As we showed in Sec. VI, if ζ_p exist and are differentiable for all real values of p, then the Gärtner-Ellis theorem ensures the large deviation principle (38). Therefore, the large deviation principle in our model is verified for any creation rate function, which has finite and differentiable moments φ_p for all real p.

We proved that the large deviation principle emerges naturally for a class of simple models of instanton creation. These models have several essential simplifications. In particular, we disregarded correlations in time and correlations between instantons in different shells. Numerical simulations show that such correlations are important. In fact, numerical values for the moments φ_p deviate strongly from the values determined by Eq. (50) for known ζ_p. Also, the function $\varphi(v)$ depends on the way it is computed. On the other hand, the numerical data provided good evidence for universality of the creation process because the function $\varphi(v)$ found numerically does not depend on the shell number n.

VIII. TURBULENT REGIME DOMINATED BY A SINGLE BLOWUP

We showed in Sec. V that the exponent y describing the universal scaling of instantons in Eq. (27) does not determine any of the scaling exponents ζ_p or their asymptotic behavior for large p; see Eq. (28) and Fig. 4. The anomalous scaling of velocity moments is linked exclusively to the process of instanton creation. In this section, we demonstrate a different turbulent regime, where the instanton scaling has a strong influence on the velocity moments. This regime can be predicted by looking at the blowup scaling exponent y_0 depending on the model parameter in Fig. 2(a). At $c = -0.139$, we have $y_0 = 0$. Hence, in the asymptotic form of blowup given by Eq. (14), all of the local maxima $v_n = \max_t |u_n(t)|$ are of the same order of magnitude. As a result, a single blowup provides the terms $(Tk_n)^{-1} v_n^{p-1} \sim k_n^{-1}$ in the sum (19) for the structure functions S'_p, which yields the condition $\zeta_p \leqslant 1$ for all p. This upper bound is exact for $\zeta_3 = 1$, which is required by the existence of energy cascade. This fact suggests that the blowup scaling should play an essential role for the Sabra models with the parameter c in the neighborhood of -0.139.

Figure 10 (thin lines and circles) shows the structure functions $S_p(k_n)$ and $S'_p(k_n)$ for $c = -0.2$ in logarithmic coordinates. Vertical shifts are used to compare the graphs for $S_p(k_n)$ and $S'_p(k_n)$, and the good match confirms the validity of the description based on velocity maxima. The inertial range shrinks substantially in this model and corresponds roughly to the shells $17 \leqslant n \leqslant 30$. In this case, the blowup scaling exponent $y_0 = 0.0534$ is small. As we just mentioned, due to a slow decay of blowup amplitudes in Eq. (14), we

expect that the inertial range is influenced by the blowup scaling.

The numerical simulation shows that a single stable instanton dominates the inertial range. This instanton is created in the initial shell $n_0 = 0$ and travels all the way to the viscous range. The bold red (gray) curves in Fig. 10 show the values of a specific term $(Tk_n)^{-1} v_n^{p-1}$ in the sum (19), which corresponds to this instanton. In the figure, we used the same vertical shift for the red curve as for the full sum $S'_p(k_n)$, which shows that not only the slope but also the value of $S'_p(k_n)$ is determined by a single instanton for large p. Due to its dominant role, this instanton is weakly influenced by surrounding fluctuations, i.e., by other instantons. As a result, we can expect that the dominant instanton scales with the same exponent y_0 as the blowup. This hypothesis agrees perfectly with the numerical data.

Figure 11 shows the scaling exponents ζ_p for the Sabra model with $c = -0.2$ and -0.139. In this case, the blowup scaling exponent is equal to $y_0 = 0.0534$ and 0, respectively; see also Fig. 2(a). The dotted straight lines in Fig. 11 show the right-hand side of the inequality (28) with $y = y_0$. We see that this inequality becomes exact for large p because of the dominant role of a single instanton. Note that the graph of ζ_p is not concave, as it must be, and violates slightly Eq. (28) in the region near the intersection with the dotted line. This seems to be a numerical artifact due to very slow convergence in the region where the blowup scaling competes with the scaling of the instanton creation process. The horizontal part of the graph with $\zeta_p = 1$ for $c = -0.139$ reminds one of the analogous behavior of scaling exponents for turbulence of the Burgers equation; see [3,7]. Our results show that there are parameter values of the Sabra model when the anomalous scaling exponents ζ_p are explicitly related to the blowup scaling exponent y_0 for some range of p.

FIG. 10. (Color online) Thin black curves present the velocity moments $S_p(k_n) = \langle |u_n|^p \rangle$ for $p = 1,3,5,7,9,11$. Circles determine the functions $S'_p(k_n)$ from Eq. (19) for the same p and even n (vertical shifts are applied to facilitate comparison with S_p). The red (bold gray) curves show the values $(Tk_n)^{-1} v_n^{p-1}$ for a single dominant instanton and $p = 5,7,9,11$.
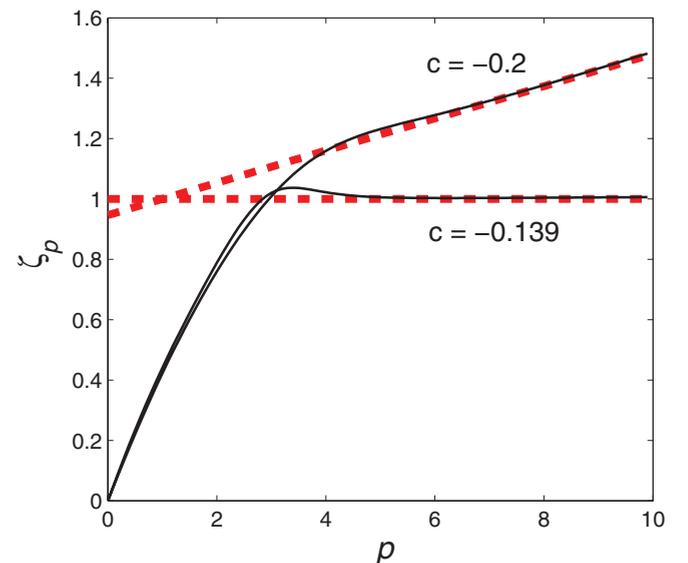
FIG. 11. (Color online) Anomalous scaling exponent ζ_p computed for the Sabra model with $c = -0.2$ and -0.139. For each case, the red dotted line shows the values of ζ_p determined by the universal scaling of a single blowup.

IX. CONCLUSION

In this paper, we have shown that the blowup (a singularity developing in finite time) may be considered as a basic element in the theory of developed turbulence for the Sabra shell model. We utilize the fact that the blowup in the inviscid system has universal asymptotic form, where shell speeds pass successively through their maxima with increasing time and wave number. This sequence of maxima is the main property used for identifying and analyzing the coherent turbulent bursts, which are induced by blowup and called the instantons.

Blowup is characterized by the asymptotically stable traveling wave solution for the renormalized system. Thus, almost any initial condition of finite norm leads to blowup in the inviscid Sabra model. In the inertial range of turbulent regime, the blowuplike structures appear in every available part of space-time and propagate toward the viscous range. This dynamical behavior can be viewed as a "gas" of instantons, which is dense in space-time and moves from the forcing to the viscous range. The existence of many interacting instantons alter their properties, as compared to the "pure" blowup, but the instanton statistics remains self-similar and universal.

We showed that the anomalous scaling of velocity moments is a natural consequence of the instanton creation process, which obeys the large deviation principle. This allows, in particular, justifying the universal form of instanton probability density functions in the inertial range and describing these universal functions analytically in terms of the scaling exponents of velocity moments. The obtained results are in excellent agreement with the numerical data.

The described dynamical picture brings us back to the famous Richardson description [30]: "Big whirls have little whirls that feed on their velocity, and little whirls have lesser whirls and so on to viscosity," which is known to be inadequate for the Navier-Stokes turbulence [2]. We see now that in the Sabra shell model, this description becomes true if one substitutes "whirls" with "instantons" (or "blowups"). The dissipation anomaly follows naturally from this picture because the instanton dynamics is unrelated to viscosity in the inertial range and the instantons move only toward large wave numbers. The intermittency becomes a simple consequence of the instanton scaling, where the scales of time and velocity are related as $\Delta t_n \sim (k_n v_n)^{-1}$. This means that large-amplitude instantons are fast, while small-amplitude instantons are slow and can be viewed as windows of low activity. We showed, however, that the described scenario is not the only possibility, and the anomalous exponents may be linked to universal properties of a single blowup for specific values of the model parameter.

The essential part of our work is based on numerical data. Here the blowup, whose properties follow from the model equations, is used as a guideline for the numerically accessible definition of instantons. If the analytical theory of turbulence for the shell model can be developed in a similar manner, the formal definition of instantons and derivation of their universal scaling properties directly from the shell model equations would be the major difficulty. An important step in this direction was done in [26], where self-similar statistics of instantons was derived as a result of the blowup interacting with small random fluctuations. Our results show that this theory should be extended by taking into account interactions among instantons and instanton creation. Note that for different shell models, the blowup structure may not be self-similar but still be universal [15], providing an extra complication. It would be interesting to test these ideas also on the cascade models of turbulence, where the interactions among variables within the same shell are introduced [20,21].

As for the 3D Navier-Stokes developed turbulence, our results confirm the common understanding of the importance of coherent structures such as, e.g., the formation of vortex filaments. The idea presented here is that it is the universal creation process of these structures that may drive turbulent dynamics in the inertial range, while the scaling of an individual structure plays a secondary role. Moreover, one may notice that such structures do not have to blow up in finite time in the inviscid limit and, e.g., the exponential rate would be sufficient. The method for identifying and tracking coherent structures from the moment of their creation until the viscous range has to be developed in order to verify our hypotheses numerically or experimentally.

ACKNOWLEDGMENT

[1] A. Kolmogorov, Dokl. Akad. Nauk SSSR **30**, 9 (1941).

[2] U. Frisch, *Turbulence: The Legacy of A.N. Kolmogorov* (Cambridge University Press, Cambridge, UK, 1995).

[3] J. Cardy, G. Falkovich, and K. Gawedzki, *Non-equilibrium Statistical Mechanics and Turbulence* (Cambridge University Press, Cambridge, UK, 2008).

[4] G. Eyink and K. Sreenivasan, Rev. Mod. Phys. **78**, 87 (2006).

[5] G. Eyink, Physica D **78**, 222 (1994).

[6] P. Constantin, E. Weinan, and E. Titi, Commun. Math. Phys. **165**, 207 (1994).

[7] E. Aurell, U. Frisch, J. Lutsko, and M. Vergassola, J. Fluid Mech. **238**, 467 (1992).

[8] J. D. Gibbon, Physica D **237**, 1894 (2008).

[9] E. B. Gledzer, Sov. Phys. Doklady **18**, 216 (1973).

[10] K. Ohkitani and M. Yamada, Prog. Theor. Phys. **89**, 329 (1989).

[11] V. S. L'vov, E. Podivilov, A. Pomyalov, I. Procaccia, and D. Vandembroucq, Phys. Rev. E **58**, 1811 (1998).

[12] L. Biferale, Annu. Rev. Fluid Mech. **35**, 441 (2003).

[13] P. Constantin, B. Levant, and E. S. Titi, Phys. Rev. E **75**, 016304 (2007).

[14] T. Dombre and J. L. Gilson, Physica D **111**, 265 (1998).

[15] A. A. Mailybaev, Nonlinearity **26**, 1105 (2013).

[16] A. A. Mailybaev, Phys. Rev. E **85**, 066317 (2012).

[17] J. L. Gilson and T. Dombre, Phys. Rev. Lett. **79**, 5002 (1997).

[18] V. S. L'vov, A. Pomyalov, and I. Procaccia, Phys. Rev. E **63**, 056118 (2001).

[19] J. Eggers and S. Grossmann, Phys. Fluids A **3**, 1958 (1991).
[20] C. Uhlig and J. Eggers, Z. Phys. B **102**, 513 (1997).
[21] C. Uhlig and J. Eggers, Z. Phys. B **103**, 69 (1997).
[22] E. D. Siggia, Phys. Rev. A **17**, 1166 (1978).
[23] T. Nakano, Prog. Theor. Phys. **79**, 569 (1988).
[24] V. S. L'vov, Phys. Rev. E **65**, 026309 (2002).
[25] A. A. Mailybaev, Phys. Rev. E **86**, 025301 (2012).
[26] I. Daumont, T. Dombre, and J. L. Gilson, Phys. Rev. E **62**, 3592 (2000).
[27] J. Gärtner, Theor. Probab. Appl. **22**, 24 (1977).
[28] R. Ellis, Ann. Probab. **12**, 1 (1984).
[29] H. Touchette, Phys. Rep. **478**, 1 (2009).
[30] L. F. Richardson, *Weather Prediction by Numerical Process* (Cambridge University Press, Cambridge, UK, 2007).